FULL PAPER – A HYBRID ELASTIC METAMATERIAL WITH TUNABLE BENDING STIFFNESS

Yangyang Chen[1], Gengkai Hu[2] and Guoliang Huang[1]

[1] Department of Mechanical and Aerospace Engineering, University of Missouri, Columbia, MO, 65211, USA, Email: yc896@mail.missouri.edu, huangg@missouri.edu, Web: http://cmdl.missouri.edu/
[2] School of Aerospace Engineering, Beijing Institute of Technology, Beijing, 100081, China, Email: hugeng@bit.edu.cn, Web: http://www.micromechanics.cn

Keywords: Elastic metamaterial; Tunable bending stiffness; Programmable wave control

ABSTRACT

Achieving vibration and/or wave attenuation with locally resonant metamaterials has attracted a great deal of attention due to their frequency dependent negative effective mass density. Moreover, adaptive phononic crystals with shunted piezoelectric patches have also demonstrated a tunable wave attenuation mechanism by controlling electric circuits to achieve a negative effective stiffness. In this paper, we propose an adaptive hybrid metamaterial that possesses both a negative mass density as well as an extremely tunable stiffness by properly utilizing both the mechanical and electric elements. The tunable wave manipulation abilities are investigated and revealed in terms of both the effective negative mass density and/or bending stiffness of the hybrid metamaterial. The programmed flexural wave manipulations and broadband negative refraction are then illustrated through three-dimensional (3D) multi-physical numerical simulations in hybrid metamaterials. Our numerical results demonstrate that the flexural wave propagation can essentially be switched between "ON/OFF" states by connecting different shunting circuits.

1 INTRODUCTION

Acoustic/elastic metamaterials are artificially engineered materials composed of subwavelength microstructures that behave like a continuous medium with unusual effective properties. Because of their enhanced range of dynamic material properties, acoustic/elastic metamaterials possessing double-negative properties have been realized by designing microstructural units with built-in monopolar and dipolar resonators, respectively, for emerging applications such as elastic wave superlenses, subwavelength imaging and acoustic cloaking [1-3]. Unfortunately, the microstructural designs required to achieve double negative properties are notably more complicated than their single negative-property counterparts. The main challenge consists of identifying a single building-block that exhibits multiple types of resonances simultaneously. The major limitation of the current acoustic/elastic metamaterial designs with mechanically resonant mechanisms is that the frequency range of the single and/or double negative properties is fixed and limited to a narrow frequency band. This inherent limitation makes their use in practical engineering applications difficult. One of the most significant challenges in acoustic/elastic metamaterial development is the ability to tune their performance without requiring physical microstructural modifications.

There has been a growing effort to explore adaptive or active acoustic/elastic metamaterial designs capable of overcoming the challenges described above and increase their effectiveness in relevant applications. By integrating adaptive or smart materials into the meta-structure, the effective properties of the adaptive metamaterial can be tuned or adapted electronically for increasingly complex systems. Among currently available adaptive materials, shunted piezoelectric materials provide an ideal platform to tune and control elastic/acoustic properties of a metamaterial in a compact way. The piezoelectric shunting technique was first introduced by Forward (1979) to damp mechanical vibrations in optical systems [4], while Hagood and von Flotow (1991) provided the first analytical formulation for the passive electrical shunts [5]. Since their pioneering works, an array of electrical shunting designs have been proposed to improve the acoustic and dynamic mitigation performance of

structures. In these works, piezoelectric components connected to inductor-resistor (LR) shunt circuits appear as a promising passive technique for noise and vibration control in dynamic structures [6-10]. This type of shunt generates an electrical resonance in the piezoelectric patch. If this electrical resonance is tuned to one of the structural modal frequencies, a considerable damping effect of the corresponding mode can be achieved. As another type of shunting strategy to enlarge the wave attenuation region, negative capacitance shunts have been proposed and investigated [11-13]. Theoretically, the negative capacitance of the shunting circuit eliminates the piezoelectric patch's inherent capacitance such that the remaining resistance can optimally convert acoustic and/or elastic wave energy in a broadband frequency region. The applications of periodic piezoelectric patches with negative capacitance shunts have also been proposed for various spatial wave control, which include the flexural wave focusing [14], adaptive wave filtering with tunable Kirigami lattices [15], and wave directionality manipulations [16]. In addition, Chen et al. implemented the negative capacitance piezoelectric shunting method into meta-structures to actively tune the locally resonant frequencies of mechanical resonators by modifying the stiffness of the resonant microstructure [17]. However, in the previous active/adaptive metamaterial design [18,19], attention is focused primarily on the frequency tunability of the negative mass density by introducing variable stiffness components into the resonators.

In this paper, we will propose a new class of adaptive hybrid metamaterials by integrating negative capacitance shunted piezoelectric patches into a passive locally resonant metamaterial, in which the negative effective mass density mechanism produced by the passive metamaterial and extremely tunable effective bending stiffness from the piezoelectric components are used in parallel. By incorporating both wave control mechanisms simultaneously, the active phononic crystal can be used to actively "enhance" or "eliminate" (switch ON/OFF) the wave attenuation properties while also allowing for the control of the double negative material properties over an extremely broad frequency range. The switchable bandgap and the broadest negative refraction region controlled by electric circuits are quantitatively characterized and interpreted by dynamic effective parameters (effective mass density and bending stiffness) to illustrate the underlying wave control mechanism. Finally, three-dimensional (3D) multi-physical wave analyses on a finite hybrid metamaterial beam and plates are conducted to validate the tunable wave propagation manipluation. The proposed hybrid metamaterial could significantly impact research areas including tunable or switchable low-frequency wave/vibration attenuation, wave guiding, wave imaging and various other wave control applications.

2 DESIGN OF THE ADAPTIVE HYBRID METAMATERIAL BEAM

This study explores the array of potential applications offered by integrating a locally resonant passive metamaterial microstructure with an adaptive phononic crystal to construct a new adaptive hybrid metamaterial and achieve adaptive wave control as illustrated in Fig. 1. The locally resonant passive metamaterial component is created by bonding a periodic array of rubber disks (working as springs) and metal cylinders (working as lumped masses) onto the surface of a host beam as shown in Fig. 1(a) for wave attenuation at subwavelength frequency region. Next, the adaptive phononic beam component is constructed with a periodic array of piezoelectric patches shunted with negative capacitance controlling circuits as shown in Fig. 1(b). Finally, the adaptive hybrid metamaterial beam is physically realized by combining these two microstructural designs as shown in Fig. 1(c). In the design, the shunted piezoelectric patches and the mechanical resonators are equally spaced with the origins of the resonators and piezoelectric patches located in the same position. The negative capacitance of the shunting circuits is denoted as c_N. The fundamental concept behind this design is the integration of the extreme bending stiffness tunability (softening, hardening, and negative stiffness) provided by the shunted piezoelectric patches with the negative mass density mechanism of the passive metamaterial. By combining both wave control mechanisms into a single system, tunable wave manipulation and control including negative refraction over a broad frequency range can be achieved in real-time and without physical modification of the microstructures. To demonstrate how the hybrid metamaterial behaves for different values of negative capacitances at different frequencies and understand the intrinsic physics and working mechanisms, an analytical model is developed [20].

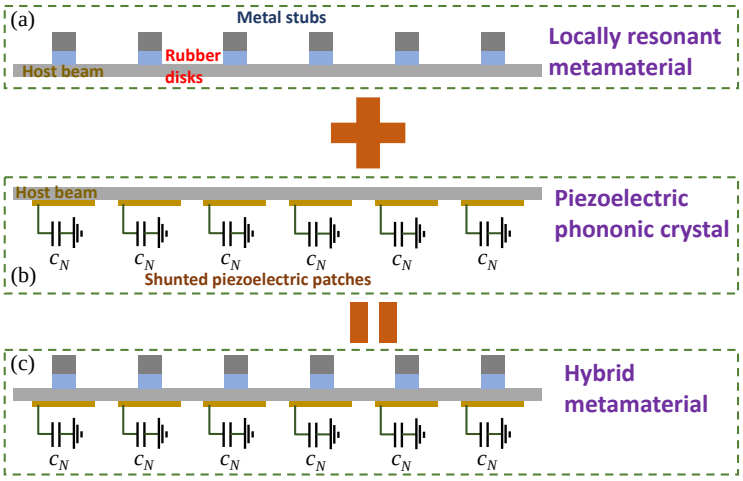

Figure 1: (a) Schematic of the passive locally resonant metamaterial beam. (b) Schematic of the adaptive piezoelectric phononic beam. (c) Schematic of the proposed adaptive hybrid metamaterial beam.

3 RESULTS AND DISCUSSION

In this section, the effective mass density and effective bending stiffness of the adaptive hybrid metamaterial beam are first analytically calculated and validated by numerical simulations. Then, the dispersion curve of the adaptive hybrid metamaterial beam is investigated for its tunable wave manipulation properties and elucidated using the effective material parameters obtained. Finally, the tunable wave control capabilities are illustrated and examined by conducting multi-physical wave propagation simulations in the finite hybrid metamaterial beam and plates.

3.1. Effective material parameters of the metamaterial beam

Effective properties of the passive metamaterial and adaptive phononic crystal are initially studied, which will be used as the foundation for conceiving the adaptive hybrid metamaterial system. Figure 2(a) shows the normalized effective mass density of a passive metamaterial beam (as shown in Fig. 1(a)) calculated analytically and numerically over frequencies of interest. In the study, the material and geometric parameters of the host beam are listed in Tab. 1, and the width is selected as 20 mm. The spring constant and weight of the mechanical resonator in the model are selected as 1×10^5 N/m and 5×10^{-3} kg, respectively. In the figure, the normalized frequency Ω is defined as ω/ω_0, where ω_0 is the resonant frequency of the mechanical resonator. The simulation results presented in Fig. 2 are performed using COMSOL Multiphysics utilizing the same 2D geometric and boundary conditions as those used in the analytical model. It can be observed from Fig. 2(a) that the analytical and numerical results are in excellent agreement, which confirms the validity of the effective mass density calculations in the analytical model. As expected, the normalized effective mass density of the passive metamaterial becomes negative at the normalized frequencies between 1 and 2 (shaded area), due to the out-of-phase motions of the resonator and host beam. It should be mentioned that the effective material parameter calculations in this study are based on the subwavelength assumption. Figure 2(b) shows the normalized effective bending stiffness of an adaptive phononic beam (as shown in Fig. 1(b)) with different uniformly shunted negative capacitances for an array of PZT-5H patches using both the analytical and numerical approaches at 10 Hz. In the figure, D_0 denotes the bending stiffness of the host beam and the material and geometric parameters listed in Tab. 1. Both the analytical and numerical results demonstrate that the normalized effective bending stiffness can gradually decrease (soften) while approaching zero before becoming negative by decreasing the negative capacitance (shaded area). After the normalized effective bending stiffness passes through its pole, it will decrease from the extremely large value (hardening) to the open circuit value. Again, very reasonable agreement can be found where the minor difference for the pole position's prediction is caused by the relatively small unit cell length-to-thickness ratio (which is 7.7 for the case in Fig. 2(b)), in which the

Euler-beam assumption is still employed. It should be mentioned that, when the unit cell length-to-thickness ratio is greater than 12, the analytical and numerical results will have an excellent agreement according to our results. The bending stiffness variation due to the negative capacitance such as stiffness softening (even negative) and hardening will be harnessed for the design of the hybrid metamaterial.

Geometric parameters (mm)			
L_b	20.0	L_p	18.0
h_b	1.6	h_p	1.0
Material properties (Host beam: Aluminum)			
E_b	70.0 GPa	b	0.33
ρ_b	2700.0 kg/m3		
Material properties (Piezoelectric patch: PZT-5H)			
c_{11}^E	126.0 GPa	e_{15}	17.0 C/m2
c_{12}^E	79.5 GPa	e_{31}	-6.55 C/m2
c_{13}^E	84.1 GPa	e_{33}	23.3 C/m2
c_{33}^E	117.0 GPa	ε_{11}^S	1700.0 ε_0
c_{44}^E	23.0 GPa	ε_{33}^S	1470.0 ε_0
c_{66}^E	23.25 GPa	ρ_p	7600.0 kg/m3

Table 1. Geometric and material parameters of the passive locally resonant metamaterial beam and adaptive piezoelectric phononic beam.

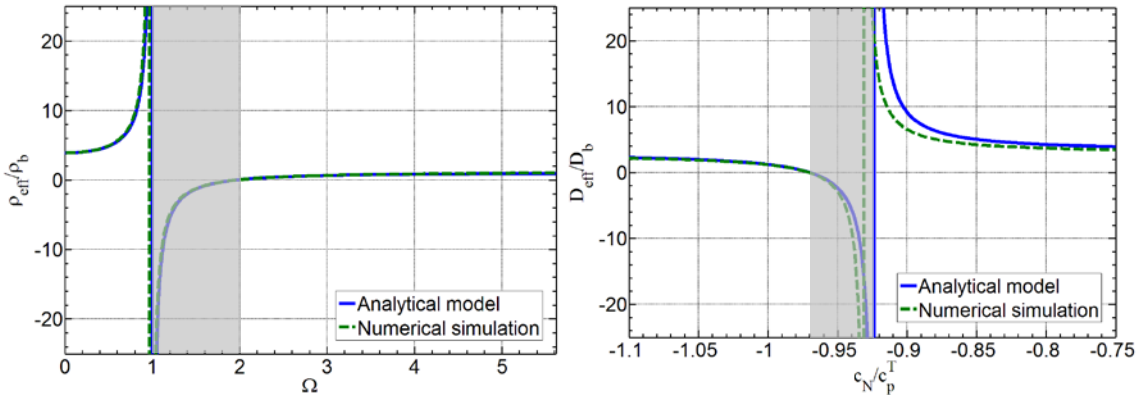

(a) (b)

Figure 2: (a) Normalized effective mass density of the passive locally resonant metamaterial beam at different frequencies. (b) Normalized effective bending stiffness of the adaptive piezoelectric phononic beam with different negative capacitance shunting circuits.

Figure 3 shows the normalized effective mass density and bending stiffness of the hybrid metamaterial (Fig. 1(c)) with short-circuit and three different negative capacitance circuits, which represent the softening, negative and hardening effective bending stiffness of the host medium based on the results presented in Fig. 2(b). In the study, the material and geometric parameters are the same as those used in Fig. 2 for the locally resonant metamaterial and piezoelectric phononic beam. As shown in Fig. 3(a) when the short circuit boundary condition is applied to the PZT patch, the negative effective mass density due to the out-of-phase motion of the resonator (shaded area) is still found but in a much narrower frequency range (1.0 ~ 1.45) than that in Fig. 2(a). This is because the attached piezoelectric patch increases the weight of the host medium. Furthermore, it is interesting to note that the effective bending stiffness is almost constant over most of the frequency region but can be significantly affected by the transverse motion of the resonator when the frequency is close to the resonant frequency. As illustrated in the figure, when the frequency approaches the resonant frequency, the effective bending stiffness of the metamaterial will dramatically decrease to negative

values in a very narrow frequency range (shaded area), then jump to large positive values after passing by the resonant frequency. After that, the effective bending stiffness will return rapidly to a constant value. The mechanism for forming the negative bending stiffness will be studied in greater detail later by conducting wave mode analysis. Figure 3(b) shows the effective property variation of the hybrid metamaterial for the case of stiffness softening of the shunted piezoelectric patch where the negative capacitance is selected as $c_N / c_p^T = -0.971$. By comparing the results in Figs. 3(a) and (b), it can be found that both the magnitude and the shape of the normalized effective mass density is not very sensitive to the change of the effective stiffness. This is because the effective mass density is primarily caused by the local transverse motion of the resonator. However, the normalized effective bending stiffness of the hybrid metamaterial is significantly reduced by simply "shearing" the effective bending stiffness to a lower value, compared with results in Fig. 3(a). As a result, the normalized frequency region of the negative effective bending stiffness induced by the resonant motion (shaded area at lower frequencies) is enlarged to 0.82 ~ 1.0, and another negative effective bending stiffness region is found at normalized frequencies higher than 2.7 (shaded area at higher frequencies). However, the frequency regions of the negative effective mass and the negative effective bending stiffness do not overlap. Figure 3(c) shows the effective properties of the hybrid metamaterial for the case of the negative stiffness of the shunted piezoelectric patch where the negative capacitance is selected to be $c_N / c_p^T = -0.95$. As expected, the effective mass density is the same as the results shown Figs. 3(a) and (b). However, the effective bending stiffness is shifted to further negative values at almost all frequencies (shaded areas). As a result, the frequency region of negative effective mass is now completely immersed in the broad frequency region of the negative effective bending stiffness. Therefore, the double negative material parameters of the hybrid metamaterial are achieved over the broadest range of frequencies. Figure 3(d) shows the effective properties of the hybrid metamaterial for the case of stiffness hardening where the negative capacitance is selected to be $c_N / c_p^T = -0.9225$. In this case, the effective bending stiffness becomes a very large positive value at almost all frequencies. More specifically, the normalized effective mass density and bending stiffness as functions of both frequency and negative capacitance values are quantitatively illustrated in Fig. 4. The color bars in the figure denote the values of normalized effective material parameters. As shown in Fig. 4(a), the negative effective mass density frequency region is not sensitive to the change of the negative capacitances. However, the normalized effective bending stiffness is primarily influenced by the negative capacitance, and will be affected by the resonator when the frequency is close to the resonant frequency. By properly harnessing electric and mechanical elements, the proposed hybrid metamaterial would possess different material properties by combining the negative effective mass density with extremely soft, hard and even negative effective bending stiffness, respectively.

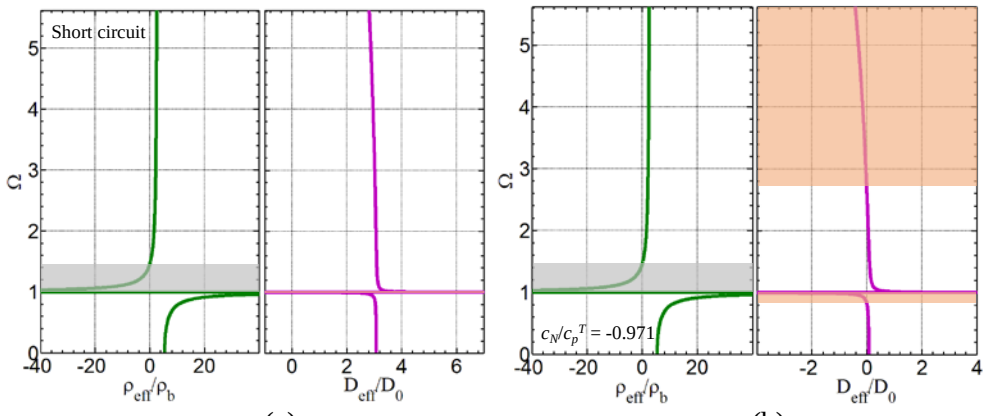

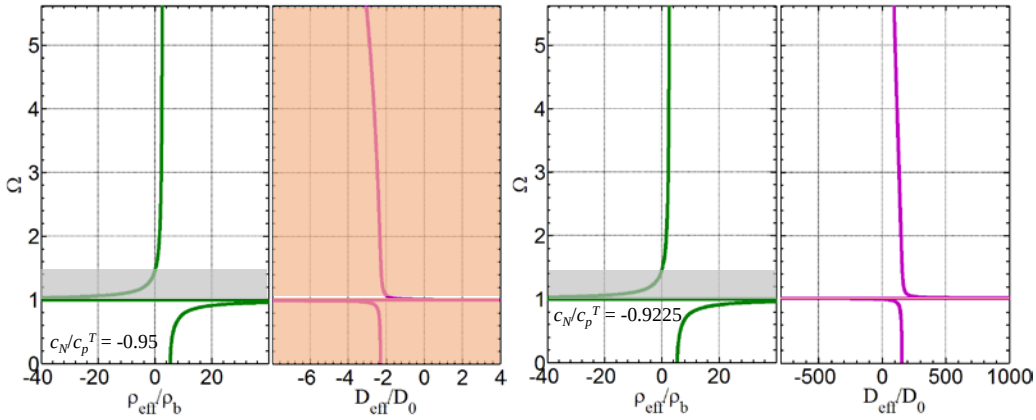

Figure 3: Normalized effective mass density and bending stiffness of the adaptive hybrid metamaterial beam with different negative capacitance shunting circuits: (a) short circuit, (b) c_N/c_p^T = -0.971, (c) c_N/c_p^T = -0.95, (d) c_N/c_p^T = -0.9225.

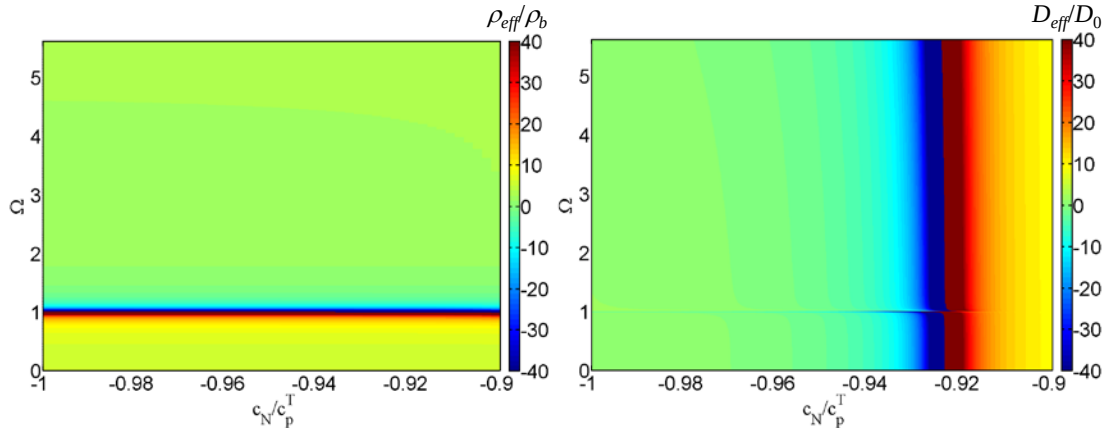

Figure 4: Normalized effective material parameters of the adaptive hybrid metamaterial beam in functions of the frequency and negative capacitance: (a) Normalized effective mass density, (b) Normalized effective bending stiffness.

3.2. Tunable wave dispersion analysis of the metamaterial beam

Figure 5 shows the complex band structures for flexural waves in the hybrid metamaterial with short-circuit and three different negative capacitance circuits which represent the bending stiffness softening, hardening and becoming negative as discussed in Fig. 3. The material, geometric and negative capacitance parameters are also left unchanged from those used in Fig. 3. As shown in Fig. 5(a) when the hybrid metamaterial is connected to a short-circuit, the imaginary part of the wavenumber in the complex band is not equal to zero at normalized frequencies from 1.0 to 1.45 (shaded area) indicating a complete band gap frequency region. In this case, the hybrid metamaterial behaves like a conventional passive metamaterial based on the local resonance mechanism. To understand the wave attenuation mechanism, the resulting subwavelength band gap frequency region is also compared with the frequency-dependent effective mass density and bending stiffness of the hybrid metamaterial beam shown in Fig. 3(a). It is found the band gap behavior is mainly caused by the negative mass density due to the out-of-phase motion of the mechanical resonator (shaded area). Figure 5(b) shows the complex band structure of the hybrid metamaterial for the softened bending stiffness where the negative capacitance is selected to be $c_N/c_p^T = -0.971$. As shown in the figure, besides the local resonance band gap, two subwavelength Bragg band gaps are found below and above the resonant band gap (shaded areas), with the normalized frequencies from 0.83 and 2.7, respectively.

It should be mentioned that the lower Bragg band gap in the complex band structure is combined with the resonant band gap forming an entirely new band gap region (shaded area), which significantly enhances the wave attenuation at much lower frequencies. In addition, the attenuation constant at the resonant band gap is much larger than in case of the short-circuit metamaterial (Fig. 3(a)). Compared with the frequency-dependent effective mass density and bending stiffness of the hybrid metamaterial beam shown in Fig. 3(b), it is found the resonant band gap is still caused by the negative effective mass density due to the out-of-phase motion of the resonator (shaded area in Fig. 3(b)). It should be noticed that the local resonance induces not only a negative effective mass but also an extremely large mass just below the resonant frequency, due to the in-phase motion of the resonator. The large mass results in strong spatial oscillation of wave fields within the periodic structures, giving rise to the Bragg gap [21]. This low-frequency Bragg gap might be different from the common one at high-frequencies because the Bragg resonance is occurring in the sub-wavelength scale, and it is related to the local resonances in the metamaterial [21]. This directional low frequency Bragg band gap induced by the local resonance has also been discussed in other literatures [22,23]. Figure 5(c) shows the complex band structure of the hybrid metamaterial for the negative bending stiffness where the negative capacitance is selected to be $c_N/c_p^T = -0.95$. The resulting stop bands occupy almost the entire range of frequencies (shaded area) and a passing band with negative phase velocity is observed between the two stop bands. In the two stop band regions, the magnitude of the real and imaginary parts of the wavenumber are almost identical due to the solution feature of the bi-harmonic governing equation of the flexural wave. To explain the wave behavior, the complex band structure is also compared with the effective mass density and bending stiffness predicted in Fig. 3(c). It is found the wave attenuation in the two stop bands is caused by the negative effective bending stiffness of the hybrid metamaterial, and the pass band with negative refraction is due to simultaneously negative effective mass density and bending stiffness. It can be observed that the frequency region of the negative refractive index is almost the same as the frequency region of the negative mass density, which cannot be produced in any passive double negative metamaterial because the frequency region of the negative modulus band is usually very narrow compared with that of the negative mass density. Figure 5(d) shows the complex band structure of the hybrid metamaterial with an extremely positive bending stiffness where the negative capacitance is selected to be $c_N/c_p^T = -0.9225$. Although the complex band structure is similar to that shown in Fig. 5(a) for the metamaterial with short circuits, the magnitude of the imaginary part of the wavenumber (attenuation constant) is significantly smaller than that in Fig. 5(a) at the normalized frequencies from 1.0 to 1.45 (shaded area). This indicates that the wave attenuation and/or stop band due to both the resonant motion and Bragg scattering mechanisms has nearly vanished or been switched OFF by the stiffness hardening shown in Fig. 3(d).

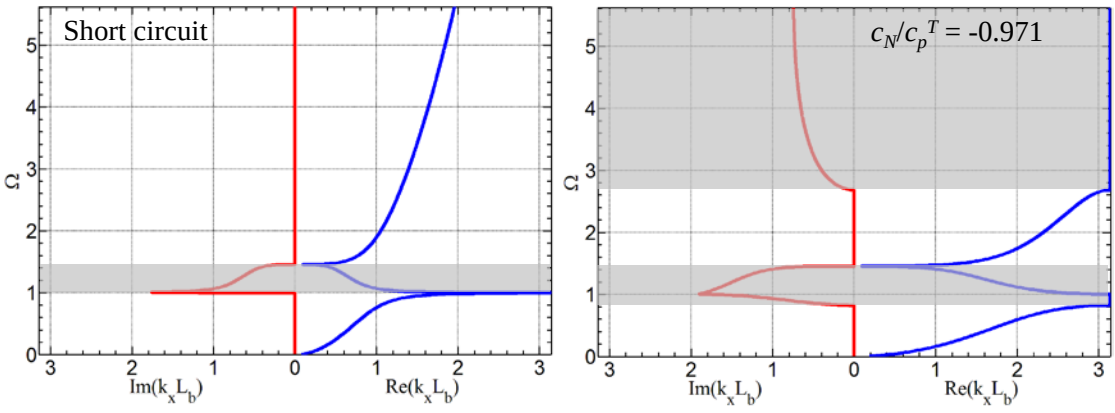

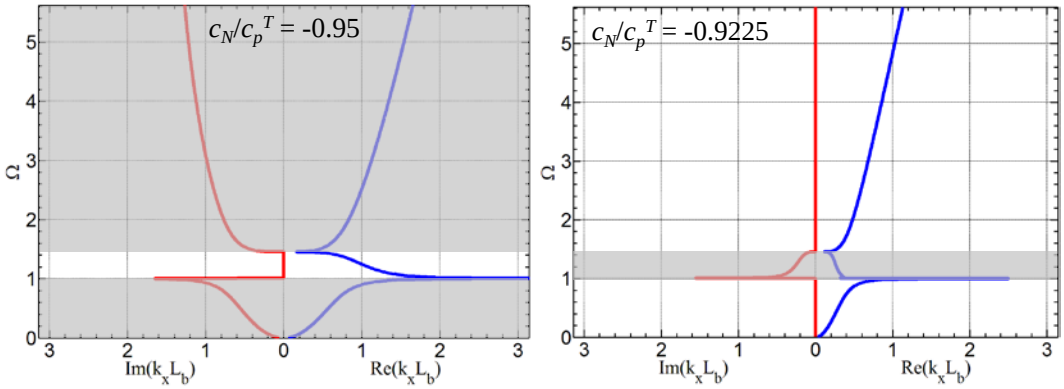

(c) (d)

Figure 5: Complex band structures of flexural waves in the adaptive hybrid metamaterial beam with different negative capacitance shunting circuits: (a) short circuit, (b) c_N/c_p^T = -0.971, (c) c_N/c_p^T = -0.95, (d) c_N/c_p^T = -0.9225.

To characterize the wave propagation behavior, complex wave dispersion relations of the hybrid metamaterial are plotted in Fig. 6 as a function of both the wave frequency and negative capacitance. The color bars in the figure denotes the values of the real and imaginary parts of the complex wavenumber. Based on the contour value of the wavenumber, the unusual and tunable wave attenuation/manipulation properties controlled by the negative capacitance can be artificially classified into five regions. Typically, in regions 1 and 5, the adaptive hybrid metamaterial beam exhibits a resonant-based band gap behavior as that in the passive metamaterial beam, where waves with normalized frequency between 1.0 and 1.45 will be attenuated. In the region 2, the resonant-based band gap is significantly enhanced by coupling with the lower-frequency Bragg band gap. However, the wave characterization in the region 3 is almost opposite to those in the regions 1 and 5 where a pass band is apparent in the original stop band frequency region, and the original pass bands are switched to stop bands. The most important aspect is that the broadest frequency region of a negative refractive index is found in this region. Finally, in region 4 the wave attenuation ability of the hybrid metamaterial is almost entirely switched OFF. The wave manipulation characteristics in the five regions will be further examined with 3D numerical simulations in the following section.

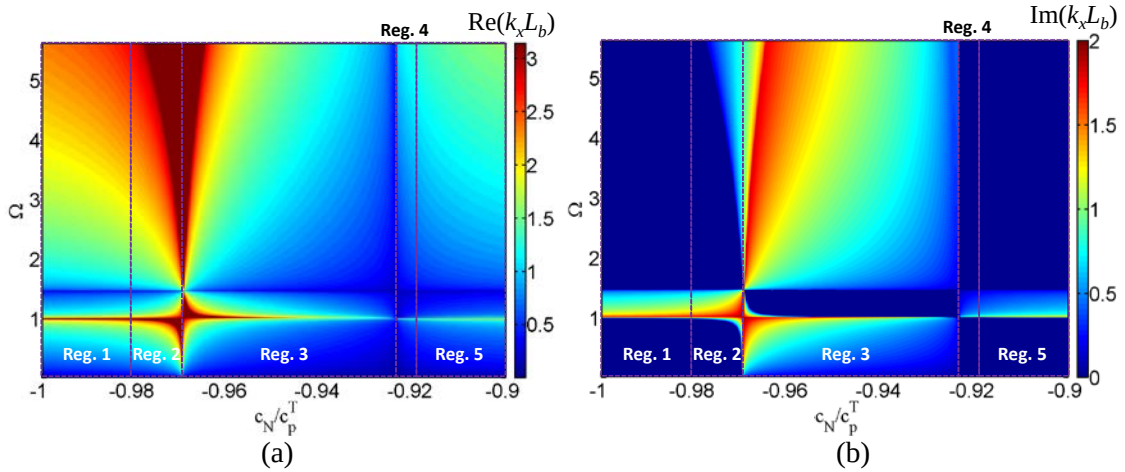

(a) (b)

Figure 6: Complex flexural wave dispersion relations of the adaptive hybrid metamaterial beam in function of the frequency and negative capacitance: (a) Real part of the wavenumber, (b) Imaginary part of the wavenumber.

3.3. Tunable wave transmittance of a finite metamaterial beam

In order to examine and validate the tunable wave transmission properties of the proposed adaptive hybrid metamaterial controlled by different negative capacitances as illustrated in Figs. 5 and 6, a 3D multi-physical numerical simulation of the harmonic wave transmission in the finite hybrid metamaterial is conducted. The schematic of the numerical modeling is shown in Fig. 7(a). In the simulation, the 3D linear piezoelectric constitutive law is applied to describe dynamic behaviors of the piezoelectric patch by using the commercial finite element software COMSOL Multiphysics. The piezoelectric shunting boundary condition is implemented through a weak form expression. The incident flexural wave is generated by applying a harmonic voltage across a PZT patch bonded to the host beam on the left-hand side of the metamaterial. Two perfectly-matched layers (PMLs) are attached to both ends of the host beam in order to suppress reflected waves from the boundaries. A displacement probe is defined on the host beam in the right-hand side of the metamaterial region to measure the out-of-plane displacement and calculate the wave transmittance. As shown Fig. 7(a), the height of the resonant metal cylinder and the rubber disk are represented by h_m and h_r, respectively, and the diameters of the metal cylinder and rubber disk are selected to be the same value and denoted by d_m. The materials of the host beam and piezoelectric patches used in the simulation are the same as those in used the analytical model. Other material and geometric parameters are given in Tab. 2.

Geometric parameters (mm)			
L_b	7.0	L_p	6.4
h_b	1.6	h_p	1.0
d_m	4.0	h_m	2.5
h_r	1.0		
Material properties (Stub resonator: Steel)			
E_s	210.0 GPa	ν_s	0.3
ρ_s	7650.0 kg/m$_3$		
Material properties (Disk: Rubber)			
E_r	25.0 MPa	ν_r	0.41
ρ_r	1000.0 kg/m$_3$		

Table 2. Geometric and material parameters of the proposed adaptive hybrid metamaterial beam.

Based on the numerically calculated effective bending stiffness, the normalized negative capacitances for tunable wave manipulation demonstrated in regions 2 – 4 can be easily determined as c_N/c_p^T = -0.9330, -0.9140 and -0.9105, respectively, which represent the softening, negative and hardening bending stiffness. Figure 7(b) shows the transmittance of the finite adaptive hybrid metamaterial with ten unit cells shunted with short and the three negative capacitance circuits. For the case of a short shunting circuit, a sharp wave transmission dip from 7.3 to 8.8 kHz (shaded area) is found, which will be used as the basis for the tunable wave control. It can be found that (1) the original wave attenuation region is enlarged to 7.1 ~ 8.8 kHz at lower frequencies when the normalized negative capacitance, c_N/c_p^T, is -0.933 (stiffness softening); (2) the wave characterization is almost reversed when the normalized negative capacitance, c_N/c_p^T, is -0.914 (negative stiffness) such that the original stop band is switched to a pass band with the negative phase velocity, and the original pass bands are switched to stop bands; (3) the wave attenuation due to the local resonator is almost entirely switched OFF when the normalized negative capacitance, c_N/c_p^T, is -0.9105 (stiffness hardening) and the transmittance is nearly uniform at all frequencies with some fluctuations in the original wave attenuation region (shaded area). Compared with the wave transmittance illustrated in the first and third figures in Fig. 7(b), we also notice that the wave attenuation due to the negative bending stiffness is much weaker than that from the negative mass density.

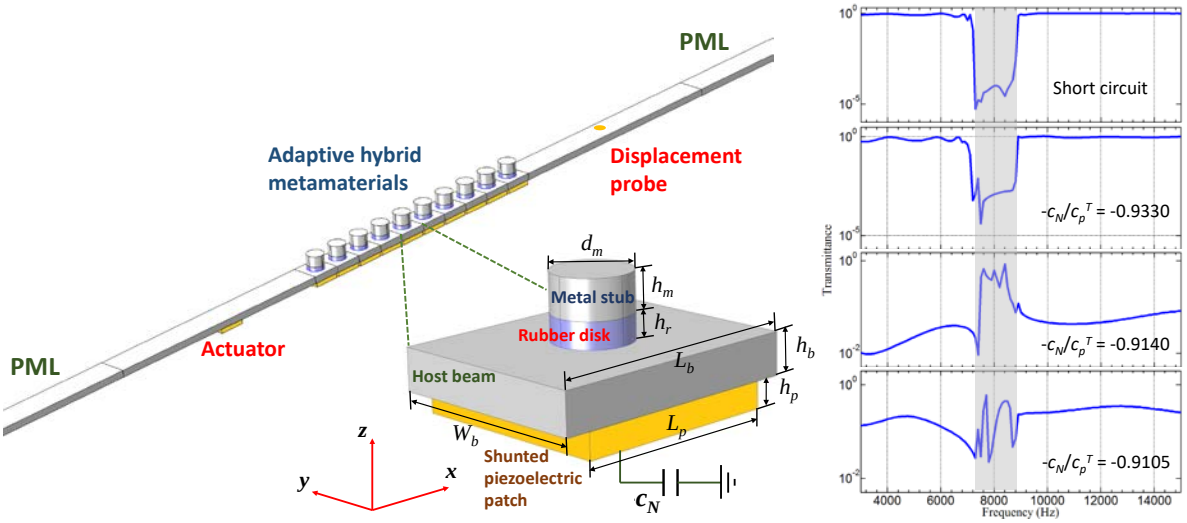

(a) (b)

Figure 7: (a) Schematic of 3D numerical simulations of the flexural wave transmission in a finite adaptive hybrid metamaterial beam. (b) Transmittance of flexural waves through an adaptive hybrid metamaterial beam with 10 unit cells with short and different negative capacitance shunting circuits.

3.4. Broadband negative refraction of a metamaterial plate

Based on the mechanism and wave behavior demonstrated in the metamaterial beam structure, the proposed adaptive hybrid metamaterial is extended into plate structures for tunable wave manipulations. Due to the broadband double negativities (negative mass density and negative bending stiffness) of the proposed metamaterial, broadband negative refraction in the entire negative mass density frequency region will be expected in the hybrid metamaterial plate. To examine this phenomenon, numerical simulations of a flat negative refraction lens composed of an array of 5×48 unit cell hybrid metamaterial plate are conducted at different frequencies. As the schematic shown in Fig. 8(a), the negative refraction lens is inclined 45° to the lower edge of the host plate, and a Gaussian flexural wave beam is incident from the left edge of the host plate to the lower part of the lens with the actuation length being 150 mm. In the harmonic numerical simulation, the PML layers are adopted to suppress reflected waves from the boundaries. The width of the host plate unit cell, w_b, is selected to be the same with L_b, and all the other geometric and material parameters are the same as those used in Fig. 7.

Figures 8(b), (c) and (d) show the normalized out-of-plane displacement wave fields of the metamaterial plate with negative effective bending stiffness (c_N/c_p^T = -0.871) at 7400, 7800, and 8200 Hz, respectively. As illustrated in Fig. 8(b), the negative refraction is observed at the two boundaries between the metamaterial and the host plate, due to the double negative material parameters at this frequency. As a result, the incident wave beam is shifted upward and propagates through the lens along the incident direction, which can be explained by applying the Snell's law twice. It should be mentioned that the wave reflection at metamaterial boundaries is quite small, as the refractive index of the metamaterial is close to the index of the host plate. The similar negative refraction phenomena are also demonstrated in Figs. 8(c) and (d). It can also be observed that with the increase of the operation frequency, the negative refractive angle becomes larger. This is because the metamaterial effective refractive index is enhanced with the decreased effective mass density and the effective bending stiffness remains being constant when the frequency is increased.

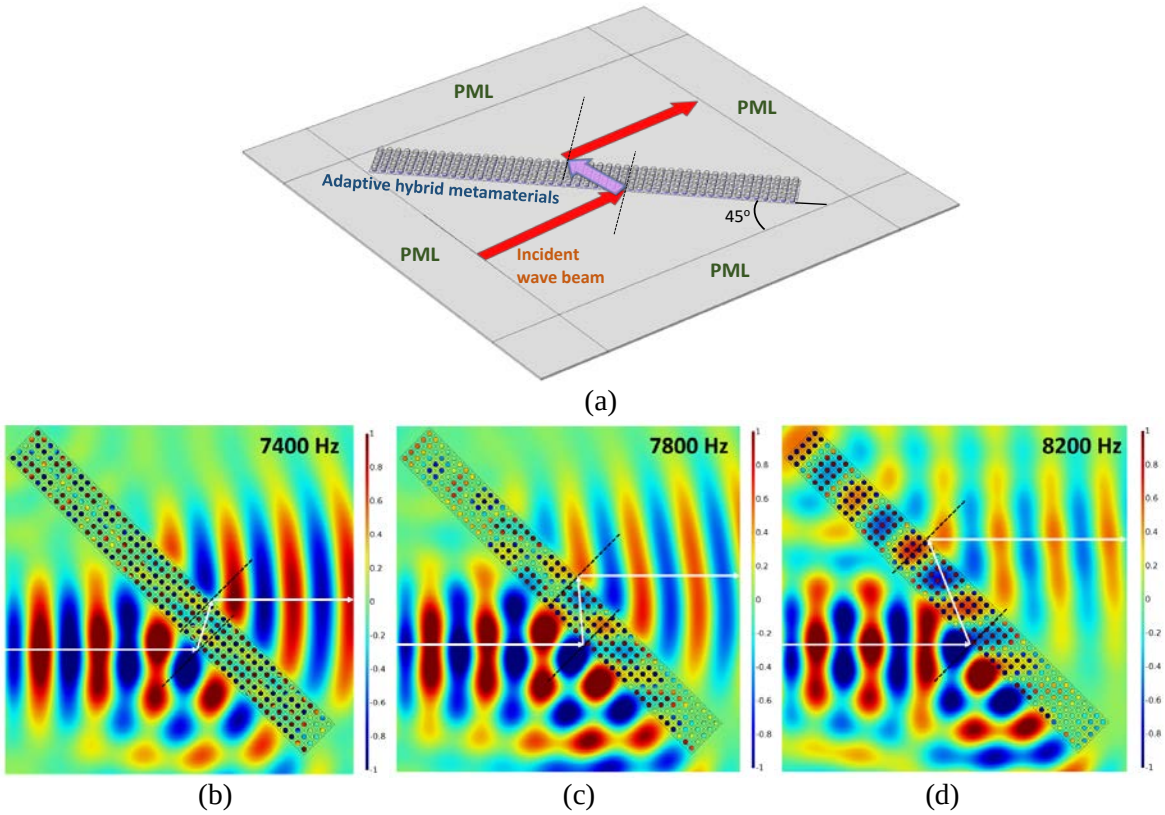

(a) (b) (c) (d)

Figure 8: (a) Schematic of 3D numerical simulations of the negative refraction in an adaptive hybrid metamaterial plate. (b-d) Normalized out-of-plane displacement fields of the adaptive hybrid metamaterial plate at different frequencies: (b) 7400 Hz, (c) 7800 Hz, (d) 8200 Hz.

4. CONCLUSIONS

In this paper, we propose an adaptive hybrid metamaterial design with negative effective mass density and extremely tunable bending stiffness by bonding an array of negative capacitance shunted piezoelectric patches into a passive locally resonant metamaterial. First, effective material parameters as well as wave dispersion relations of the hybrid metamaterial beam are derived analytically based on the developed multi-physical model which considers the locally resonant motions, electro-mechanical coupling and shunting circuitry effects. Extremely tunable wave manipulation properties of the adaptive hybrid metamaterial are interpreted by combining the negative effective mass density and extremely tunable bending stiffness. Finally, 3D numerical simulations for wave transmission and broadband negative refraction in the hybrid metamaterial are conducted. We hope that the proposed concept, design and approach can open many possibilities for tunable broadband wave/vibration attenuation, wave guiding and imaging applications, such as nondestructive evaluation and structural health monitoring.

ACKNOWLEDGMENTS

This work is supported by the Air Force Office of Scientific Research under Grant No. AF 9550-15-1-0016 with Program Manager Dr. Byung-Lip (Les) Lee.

REFERENCES

[1] X.N. Liu, G.K. Hu, G.L. Huang and C.T. Sun, An elastic metamaterial with simultaneously negative mass density and bulk modulus, *Appl. Phys. Lett.*, **98**, 2011, 251907.

[2] R. Zhu, X.N. Liu, G.K. Hu, C.T. Sun and G.L. Huang, Negative refraction of elastic waves at the deep-subwavelength scale in a single-phase metamaterial, *Nat. Commun.*, **5**, 2014, 5510.

[3] Y. Wu, Y. Lai and Z.Q. Zhang, Elastic metamaterials with simultaneously negative effective shear modulus and mass density, *Phys. Rev. Lett.*, **107**, 2011, 105506.

[4] R.L. Forward, Electronic damping of vibrations in optical structures, *J. Appl. Opt.*, **18**, 1979, 690-697.

[5] N.W. Hagood and A.V. Flotow, Damping of structural vibrations with piezoelectric materials and passive electrical networks, *J. Sound Vib.*, **146**, 1991, 243-268.

[6] L. Airoldi and M. Ruzzene, Design of tunable acoustic metamaterials through periodic arrays of resonant shunted piezos, *New J. Phys.*, **13**, 2011, 113010.

[7] S.B. Chen, G. Wang, J.H. Wen and X.S. Wen, Wave propagation and attenuation in plates with periodic arrays of shunted piezo-patches, *J. Sound Vib.*, **332**, 2013, 1520-1532.

[8] A.E. Bergamini, M. Zündel, E.A. Flores Parra, T. Delpero, T. Delpero, M. Ruzzene and P. Ermanni, Hybrid dispersive media with controllable wave propagation: a new take on smart materials, *J. Appl. Phys.*, **118**, 2015, 154310.

[9] D. Cardell, P. Celli and S. Gonella, Manipulating waves by distilling frequencies: a tunable shunt-enabled rainbow trap, *Smart Mater. Struct.*, **25**, 2016, 085017.

[10] G. Wang and S.B. Chen, Large low-frequency vibration attenuation induced by arrays of piezoelectric patches shunted with amplifier–resonator feedback circuits, *Smart Mater. Struct.*, **25**, 2016, 015004.

[11] M. Collet, M. Ouisse and M. Ichchou, Structural energy flow optimization through adaptive shunted piezoelectric metacomposites. *J. Intell. Mater. Syst. Struct.*, **23** (15), 2012, 1661-1677.

[12] B.S. Beck, K.A. Cunefare, M. Ruzzene and M. Collet, Experimental analysis of a cantilever beam with a shunted piezoelectric periodic array. *J. Intell. Mater. Syst. Struct.*, **22**, 2011, 1177-1187.

[13] F. Tateo, M. Collet, M. Ouisse, M. Ichchou, K. Cunefare and P. Abbe, Experimental characterization of a bi-dimensional array of negative capacitance piezo-patches for vibroacoustic control, *J. Intell. Mater. Syst. Struct.*, **26**, 2014, 952-964.

[14] K. Yi, M. Collet, M. Ichchou and L. Li, Flexural waves focusing through shunted piezoelectric patches, *Smart Mater. Struct.*, **25**, 2016, 075007.

[15] M. Ouisse, M. Collet and F. Scarpa, A piezo-shunted kirigami auxetic lattice for adaptive elastic wave filtering, *Smart Mater. Struct.*, **25**, 2016, 115016.

[16] Z.-W. Zhu and Z.-C. Deng, Elastic wave propagation in adaptive honeycomb-based materials with high connectivity, *Smart Mater. Struct.*, **25**, 2016, 085003.

[17] Y.Y. Chen, G.L. Huang and C.T. Sun, Band gap control in an active elastic metamaterial with negative capacitance piezoelectric shunting, *J. Vib. Acoust.*, **136**, 2014, 061008.

[18] Y.Y. Chen, G.K. Hu and G.L. Huang, An adaptive metamaterial beam with hybrid shunting circuits for extremely broadband control of flexural waves, *Smart Mater. Struct.*, **25**, 2016, 105036.

[19] R. Zhu, Y.Y. Chen, M.V. Barnhart, G.K. Hu, C.T. Sun and G.L. Huang, Experimental study of an adaptive elastic metamaterial controlled by electric circuits, *Appl. Phys. Lett.*, **108**, 2016, 011905.

[20] Y.Y. Chen, G.K. Hu and G.L. Huang, A hybrid elastic metamaterial with negative mass density and tunable bending stiffness, *J. Mech. Phys. Solids*, **105**, 2017, 179-198.

[21] A.P. Liu, X.M. Zhou, G.L. Huang and G.K. Hu, Super-resolution imaging by resonant tunneling in anisotropic acoustic metamaterials. *J. Acoust. Soc. Am.*, **132**, 2012, 2800-2806.

[22] Y. Xiao, J. Wen and X. Wen, Flexural wave band gaps in locally resonant thin plates with periodically attached spring-mass resonators, *J. Phy. D*, **45**, 2012, 195401.

[23] Y. Xiao, J. Wen, D. Yu and X. Wen, Flexural wave propagation in beams with periodically attached vibration absorbers: band-gap behavior and band formation mechanisms, *J. Sound Vib.*, **332**, 2013. 867–893.